Cell Reports

CellPress
OPEN ACCESS

Article

Phase separation-mediated condensation of Whirlin-Myo15-Eps8 stereocilia tip complex

Lin Lin,[1,2,4] Yingdong Shi,[3,4] Mengli Wang,[3] Chao Wang,[3] Qing Lu,[2] Jinwei Zhu,[1,2,5,*] and Rongguang Zhang[1,*]

[1]State Key Laboratory of Molecular Biology, Shanghai Institute of Biochemistry and Cell Biology, Center for Excellence in Molecular Cell Science, Chinese Academy of Sciences, Shanghai 200031, China

[2]Bio-X Institutes, Key Laboratory for the Genetics of Developmental and Neuropsychiatric Disorders, Ministry of Education, Shanghai Jiao Tong University, Shanghai 200240, China

[3]Ministry of Education Key Laboratory for Membrane-less Organelles & Cellular Dynamics, Hefei National Laboratory for Physical Sciences at the Microscale, School of Life Sciences, Division of Life Sciences and Medicine, University of Science and Technology of China, Hefei 230026, China

[4]These authors contributed equally

[5]Lead contact

*Correspondence: jinwei.zhu@sjtu.edu.cn (J.Z.), rgzhang@sibcb.ac.cn (R.Z.)

https://doi.org/10.1016/j.celrep.2021.108770

SUMMARY

Stereocilia, the mechanosensory organelles on the apical surface of hair cells, are necessary to detect sound and carry out mechano-electrical transduction. An electron-dense matrix is located at the distal tips of stereocilia and plays crucial roles in the regulation of stereocilia morphology. Mutations of the components in this tip complex density (TCD) have been associated with profound deafness. However, the mechanism underlying the formation of the TCD is largely unknown. Here, we discover that the specific multivalent interactions among the Whirlin-myosin 15 (Myo15)-Eps8 complex lead to the formation of the TCD-like condensates through liquid-liquid phase separation. The reconstituted TCD-like condensates effectively promote actin bundling. A deafness-associated mutation of Myo15 interferes with the condensates formation and consequently impairs actin bundling. Therefore, our study not only suggests that the TCD in hair cell stereocilia may form via phase separation but it also provides important clues for the possible mechanism underlying hearing loss.

INTRODUCTION

Usher syndrome (USH) is an autosomal recessive genetic disease characterized by deafness and vision impairment (Boughman et al., 1983; Keats and Corey, 1999; Mathur and Yang, 2019). A lot of USH causative genes have been identified during the last several decades (Michalski and Petit, 2019; Petit and Richardson, 2009). These genetic data reveal that the abnormal development of hair cells may underlie the pathogenesis of the syndrome (Barr-Gillespie, 2015). Hair cells are specialized mechanoreceptor cells that detect sound and then carry out mechano-electrical transduction (MET). The mechanosensory organelles of hair cells are hair bundles or stereocilia, a cluster of actin-rich protrusions located at the apical surface of polarized hair cells (Barr-Gillespie, 2015; Gillespie and Müller, 2009; Figure 1A). Stereocilia are organized into rows of graded heights forming precisely uniform staircase patterns, which are interconnected by various extracellular hair bundle links, such as tip links (Gillespie and Müller, 2009; Kachar et al., 2000; Richardson and Petit, 2019; Sakaguchi et al., 2009; Figure 1A). Electron microscopy (EM) analysis has revealed that the lower and upper insertion sites of tip links are electron-dense areas that are referred to as lower tip link density (LTLD) and upper tip link density (UTLD), respectively (Furness and Hackney, 1985; Gillespie and Müller, 2009; Sahin et al., 2005; Figure 1A).

Proper development and maintenance of stereocilia are essential for normal hair cell functions (Barr-Gillespie, 2015; Richardson and Petit, 2019). It is not fully understood, however, how stereocilia length is controlled. Intriguingly, several proteins encoded by USH causative genes have been involved in the regulation of actin cytoskeleton dynamics in stereocilia (Drummond et al., 2012). Deafness-associated mutations of these actin cytoskeleton regulatory proteins perturb stereocilia growth and consequently lead to hearing loss (Sahin et al., 2005). Specifically, a set of protein complexes located at the distal tips of the tallest stereocilia (also known as "tip complex"), which includes Whirlin, myosin 15 (Myo15), Eps8, LGN, and Gαi, plays crucial roles in promoting actin polymerization and bundling (Belyantseva et al., 2003, 2005; Mauriac et al., 2017; Sahin et al., 2005; Zampini et al., 2011; Figure 1A).

Myo15, an unconventional myosin expressed in cochlear hair cells, is thought to transport protein cargos within developing stereocilia (Belyantseva et al., 2005; Delprat et al., 2005). Mutations of Myo15 cause profound deafness both in humans and mice (Probst et al., 1998; Wang et al., 1998). Mice deficient in Myo15 (*shaker-2* mice) displayed very short stereocilia without

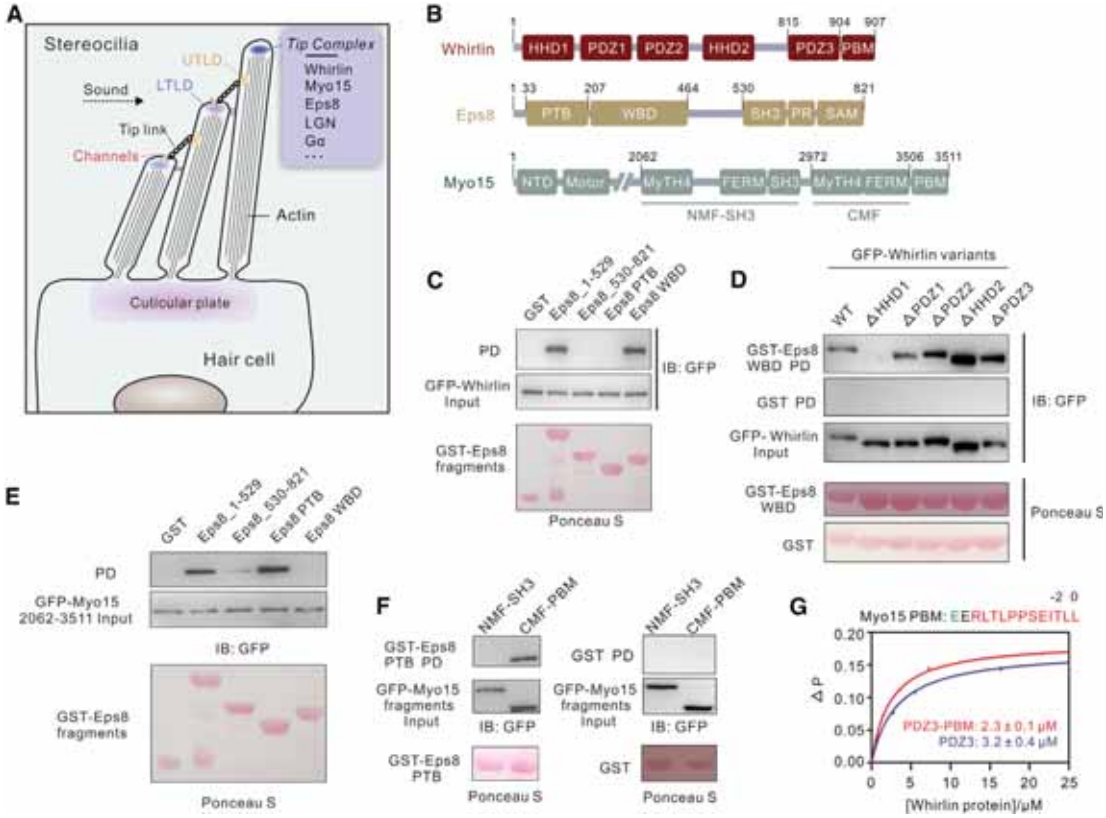

Figure 1. Characterization of interactions between Whirlin, Myo15, and Eps8

(A) A schematic diagram illustrating the organization of hair cell stereocilia.

(B) Domain organizations of key components of the tip complex in stereocilia. FERM, 4.1/ezrin/radixin/moesin; HHD, Harmonin homology domain; Myth4, myosin tail homology 4; NTD, N-terminal domain; PDZ, PSD-95/Discs-large/ZO-1 homology; PBM, PDZ binding motif; PR, proline-rich region; PTB, phosphotyrosine binding; SAM, sterile alpha motif; SH3, Src homology 3; WBD, Whirlin binding domain.

(C and D) GST-pull down assays showing that the WBD domain of Eps8 (C) and the HHD1 domain of Whirlin (D) were essential for Whirlin-Eps8 interaction. PD, pull down.

(Eand F) GST-pull-down assays showing that the PTB domain of Eps8 (E) and the CMF-PBM domain of Myo15 (F) were essential for Myo15-Eps8 interaction.

(G) Fluorescence polarization-based assays showing the binding affinities of Myo15 PBM to Whirlin PDZ3 and Whirlin PDZ3-PBM. The sequence of Myo15 PBM is also shown here with completely conserved residues colored in red and less conserved residues colored in green. All of the binding assays were repeated 3 times (N = 3). Representative experiments are shown.

See also Figure S1.

tip links (Probst et al., 1998). Whirlin (encoded by *WHRN* gene) is a USH protein that sequentially consists of N-terminal harmonin homology domain 1 (HHD1), a tandem of PDZ domains (PDZ1–2), HHD2, and the PDZ3 domain directly followed by a C-terminal PDZ-binding motif (PBM) (Mburu et al., 2003; Figure 1B). Whirlin acts as an organizer of the tip complex that control the coordinated actin dynamics of stereocilia (Kikkawa et al., 2005). Mutations of *WHRN* have been found in patients with either non-syndromic deafness (DFNB31) (Mburu et al., 2003) or USH of type 2 (USH2D) (van Wijk et al., 2006). Mice deficient in Whirlin (*whirler* mice) were profoundly deaf and showed short stereocilia (Mburu et al., 2003). Eps8 (epidermal growth factor receptor pathway substrate 8) is an evolutionarily conserved regulator of actin dynamics and can control actin-based motility by capping the barbed ends of actin filaments and promoting actin bundling (Disanza et al., 2004, 2006). In addition, Eps8 can directly interact with monomeric actin (Hertzog et al., 2010). Like *shaker-2* and *whirler* mice, *Eps8* knockout mice also exhibit similar stereocilia stunting and severe hearing loss (Zampini et al., 2011), indicating a strong genetic interaction between these three deafness-associated genes (Behlouli et al., 2014). Physically, Myo15 interacts with both Whirlin and Eps8 (Manor et al., 2011). These interactions are required for Myo15-mediated trafficking of Whirlin and Eps8 to the very tips of stereocilia (Belyantseva et al., 2003, 2005). Whirlin was also found to interact with Eps8 in the tip complex (Manor et al., 2011). Expression of both Eps8 and Myo15 at stereocilia tips was reduced in Whirlin-deficient mice (Manor et al., 2011), suggesting a critical scaffolding role of Whirlin in the assembly of the stable Whirlin-Myo15-Eps8 tip complex.

Most notably, transmission EM (TEM) images have shown that an electron-dense structure is located at the distal tips of stereocilia and covers the barbed ends of the actin protrusions (Engström and Engström, 1978; Furness and Hackney, 1985;

Hackney and Furness, 2013; Mogensen et al., 2007; Rzadzinska et al., 2004; Figure 1A). This dense structure exhibits properties reminiscent of the postsynaptic density (PSD) in neurons (Palay, 1956). PSD contains various proteins and forms a densely packed structure to regulate actin cytoskeleton dynamics in accordance with distinct neuronal stimuli (Zhu et al., 2016). Similarly, the components of the tip complex may act as key molecular organizers of this tip complex density (TCD) (Gillespie and Müller, 2009; Sahin et al., 2005). For example, the tallest stereocilia showed very strong Myo15 staining covering their oblate tips, whereas the *shaker-2* mice exhibited a rounded tip without the characteristic TCD and displayed bundle defects (Rzadzinska et al., 2004). The electron density at the tips of stereocilia was markedly patchy and irregular in the *whirler* mice (Mogensen et al., 2007). Intriguingly, the electron-dense material-free areas appeared to coincide with a lack of actin filament at the tip (Mogensen et al., 2007). These observations also suggest a tight correlation between the TCD formation and stereocilia growth. Despite the crucial roles of the tip complex-mediated formation of TCD in orchestrating the architecture and function of hair cell stereocilia, several key questions remain to be answered. What is the molecular basis underlying the assembly of the tip complex? How could the tip complex contribute to form electron-dense TCD assembly? What is the relationship between TCD formation and the pathogenesis of USH?

In this study, we characterize the interactions between Whirlin, Myo15, and Eps8 in detail and provide the high-resolution structure of the Whirlin-Myo15 complex. Importantly, we demonstrate that the formation of the Whirlin-Myo15-Eps8 complex leads to autonomous condensation of the complex both *in vitro* and in cells via liquid-liquid phase separation (LLPS). Our biochemical reconstitution experiments suggest that the key components of the tip complex are sufficient to form the densely packed TCD-like condensates. We further demonstrate that the reconstituted TCD-like condensates effectively promote actin bundling. A deafness-associated mutation of Myo15 impairs the formation of the condensates and thus leads to defects in actin bundling.

RESULTS

Characterization of the interactions between Whirlin, Myo15, and Eps8

We wanted to dissect the interactions among Whirlin, Myo15, and Eps8. A previous study reported that Whirlin binds to the N-terminal region (amino acids [aa] 1–535) of Eps8 (Manor et al., 2011). We verified this interaction by showing that glutathione S-transferase (GST)-Eps8$^{1–529}$, but not GST-Eps8$^{530–821}$, bound robustly to GFP-tagged Whirlin in the GST-pull down assays (Figure 1C). We further found that Eps8$^{207–464}$ (referred to as Whirlin-binding domain [WBD]) also bound effectively to Whirlin, whereas Eps8 phosphotyrosine binding (PTB) (aa 33–207) did not (Figure 1C). In line with our biochemical data, both RFP-Eps8$^{1–529}$ and RFP-Eps8 WBD could colocalize with GFP-Whirlin into the cytoplasmic punctate-like structures in cells, whereas red fluorescent protein (RFP)-Eps8 PTB could not (Figure S1A). Next, we wanted to dissect which domain or domains of Whirlin are required for Eps8 binding. Various deletion forms of Whirlin were introduced to test their binding to Eps8 WBD. We found that deletion of the HHD1 domain, but not other domains, completely eliminated the Whirlin-Eps8 WBD interaction (Figure 1D). These data suggested that the WBD of Eps8 and the HHD1 domain of Whirlin are essentially required for Whirlin-Eps8 interaction.

Consistent with an earlier study (Manor et al., 2011), we showed that both GST-Eps8$^{1–529}$ and GST-Eps8$^{530–821}$ bound to Myo15 tail (Myo15$^{2,062–3,511}$), although Eps8$^{1–529}$ displayed a much stronger binding than Eps8$^{530–821}$ did (Figure 1E). Myo15 tail includes the N-terminal Myth4-FERM domain (NMF), the SH3 domain, and the C-terminal Myth4-FERM domain (CMF), followed by a PBM (Figure 1B). Further truncation-based assays demonstrated that the PTB domain of Eps8 and CMF-PBM of Myo15 were the major binding sites for Myo15-Eps8 interaction (Figures 1E and 1F). Myo15 accumulates at filopodia tips when overexpressed in heterologous cells (Belyantseva et al., 2003). In line with our biochemical data, both RFP-Eps8$^{1–529}$ and RFP-Eps8 PTB could colocalize with GFP-Myo15 at the very tips of filopodia in cells, whereas RFP-Eps8 WBD could not (Figure S1B).

Myo15 was shown to bind to the third PDZ domain of Whirlin via its C-terminal evolutionarily conserved type I PBM (Belyantseva et al., 2005). We found that the interaction between Myo15 PBM and Whirlin PDZ3 was required for trafficking of Whirlin to filopodia tips via Myo15 (Figure S1C), an observation that is similar to the previous studies (Belyantseva et al., 2005; Mauriac et al., 2017). Fluorescence polarization-based assays showed that Myo15 PBM bound directly to Whirlin PDZ3 (aa 815–904) and Whirlin PDZ3-PBM (aa 815–907) with dissociation constants (K_D) of ~3.2 and ~2.3 μM, respectively (Figure 1G). The above data indicate that Whirlin, Myo15, and Eps8 can interact directly with one another, thus forming the stable tip complex (Figure S1D).

Structural basis of the Whirlin-Myo15 interaction

To investigate the molecular basis governing the Myo15-Whirlin interaction, we tried to crystallize Myo15 PBM with Whirlin PDZ3 or Whirlin PDZ3-PBM. We were able to obtain crystals of Whirlin PDZ3-PBM in complex with a synthetic Myo15 PBM peptide. We determined the complex structure at 1.7 Å resolution by the molecular replacement method (Table S1). Each asymmetric unit contains one copy of the complex. In the complex structure, Whirlin PDZ3 adopts a canonical PDZ domain architecture composed of five β strands (βA–E) and two helices (αA and αB) (Figure 2A). Myo15 PBM occupies the groove formed by αB and βB of Whirlin PDZ3 (Figure 2A). Interestingly, Myo15 PBM, in addition to forming anti-parallel β sheet pairs with βB of Whirlin PDZ3, forms parallel β sheets with the PBM of Whirlin in the neighboring asymmetric unit, indicating the tendency of oligomerization of the complex in the crystal (Figure S2A). However, the Whirlin PDZ3-PBM/Myo15 PBM complex existed as a monomer in solution according to the static light-scattering assays (Figure S2B), suggesting that the parallel β sheet binding mode observed in the crystal may be due to crystal packing artifacts.

In detail, Whirlin PDZ3 interacts with Myo15 PBM in a typical PBM-PDZ binding mode (Zhang and Wang, 2003). The side chain of L(0) of Myo15 PBM inserts into the hydrophobic pocket

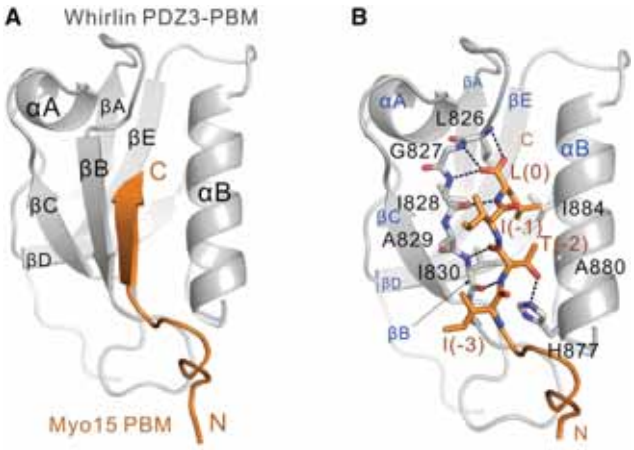

Figure 2. Crystal structure of Whirlin-Myo15 complex

(A) Overall structure of the Whirlin PDZ3-PBM-Myo15 PBM complex.

(B) Detailed interface between Whirlin PDZ3-PBM and Myo15 PBM. Residues involved in protein interaction are shown with the stick model. Hydrogen bonds are shown as black dashed lines.

See also Figure S2 and Table S1.

formed by L826, I828, I830, and I884 from Whirlin PDZ3. The carboxyl group of L(0) of Myo15 PBM forms hydrogen bonds with the backbone amides of L826, G827, and I828 (the "GLGF" motif of PDZ domain) of Whirlin PDZ3. The side chain of T(−2) of Myo15 PBM interacts with the imidazole ring of H877 at the αB helix of Whirlin PDZ3 (Figure 2B).

Whirlin undergoes phase separation *in vitro* and in living cells

An interesting observation during our cellular imaging study was that GFP-Whirlin formed bright puncta in cytosol when expressed in cells (Figure 3A). A fluorescence recovery after photobleaching (FRAP) experiment showed that GFP-Whirlin signals could be recovered after photobleaching over a short period of time (Figures 3A and 3B), suggesting that GFP-Whirlin could exchange between the puncta and the surrounding cytoplasm. These data indicated that the puncta were reversible liquid droplets. We purified the recombinant full-length Whirlin protein and found that Whirlin protein became turbid at room temperature when the concentration was >20 μM and turned clear again after being cooled on ice. Under differential interference contrast (DIC) microscopy, the turbid solution formed many spherical liquid droplets (Figure 3C). Moreover, Cy3-labeled Whirlin protein forms bright droplets in solution in a concentration-dependent manner under fluorescence microscopy (Figure 3C). These droplets could fuse with one another into larger spherical droplets over time (Figure 3D). The FRAP experiment showed that the recombinant the Cy3 signals could recover after photobleaching as well, suggesting that Whirlin could exchange between the droplets and the surrounding solution (Figure 3E). We further tested the ability of Whirlin to form liquid droplets in buffers with different salt concentrations. Significantly, both the size and number of the droplets were reduced when the NaCl concentration was elevated (Figure 3F). The above biophysical features of Whirlin are reminiscent of biomolecular condensates formed via LLPS (Banani et al., 2017; Hyman et al., 2014; Shin and Brangwynne, 2017), suggesting that Whirlin can autonomously undergo phase separation *in vitro* and in living cells. Previous reports demonstrated that Whirlin can form oligomers (Chen et al., 2014; Delprat et al., 2005). More specifically, HHD1-PDZ1 was found to bind to itself as well as to PDZ2, and PDZ3 was also found to bind to itself (Chen et al., 2014). One would thus expect that these multivalent intermolecular interactions in Whirlin may contribute to its phase separation. In line with this hypothesis, a short isoform of Whirlin (Whirlin^{short}), which lacks the HHD1, PDZ1, and PDZ2 domains, could not form phase separation (Figure S4).

Formation of Whirlin-Myo15-Eps8 complex leads to TCD-like condensates

The fact that Whirlin, Eps8, and Myo15 interact specifically with one another may allow Whirlin-Myo15-Eps8 complex to form open oligomers (see below), thus promoting the formation of the liquid-like condensates. To verify this hypothesis, we decided to reconstitute the Whirlin-Myo15-Eps8 complex *in vitro*. We tried to purify recombinant full-length Myo15 and Eps8. However, we failed to obtain soluble full-length Myo15 protein. Alternatively, we successfully purified a truncated Myo15 protein (Myo15 CMF-PBM), which includes both binding sites for Whirlin and Eps8 (Figure 3A). Although we could purify full-length Eps8 protein, the amount was relatively limited, which is not suitable for extensive phase separation study. Instead, we were able to obtain large amounts of a truncated Eps8 (Eps8 PTB-WBD), which includes both binding sites for Whirlin and Myo15 (Figure 4A). For simplicity, we referred to these two truncated proteins as Myo15 and Eps8, respectively, during our subsequent reconstitution experiments.

When mixing fluorescently labeled Whirlin, Myo15, and Eps8 at a 1:1:1 molar ratio, we observed micrometer-sized, condensed droplets with spherical shapes under fluorescence microscopy (Figure 4B). Each droplet was enriched with all three proteins. Importantly, the number and size of the droplets progressively reduced when the concentration of the complex decreased (Figure 4B). Notably, the addition of Myo15 and Eps8 significantly lowered the threshold concentration of phase separation to ≤5 μM (Figures 4B versus 3C). The FRAP experiment suggested that each protein could exchange between the condensed phase and the aqueous solution (Figure 4C). Consistently, the three proteins could perfectly colocalize with each other into bright spherical puncta when they were co-expressed in cells (Figure 4D). The intensities of each protein in the cytoplasmic puncta could recover after photobleaching over a short period of time (Figure 4E). Notably, the recovery rate of Whirlin in the TCD-like condensates is much slower than that of Whirlin alone, suggesting that the TCD-like condensates may be highly dense and less dynamic.

Although the biomolecular condensates are in general driven by low-complexity sequences of intrinsic disordered regions (IDRs) (Banani et al., 2017; Shin and Brangwynne, 2017; Wright and Dyson, 2015), specific and multivalent protein-protein

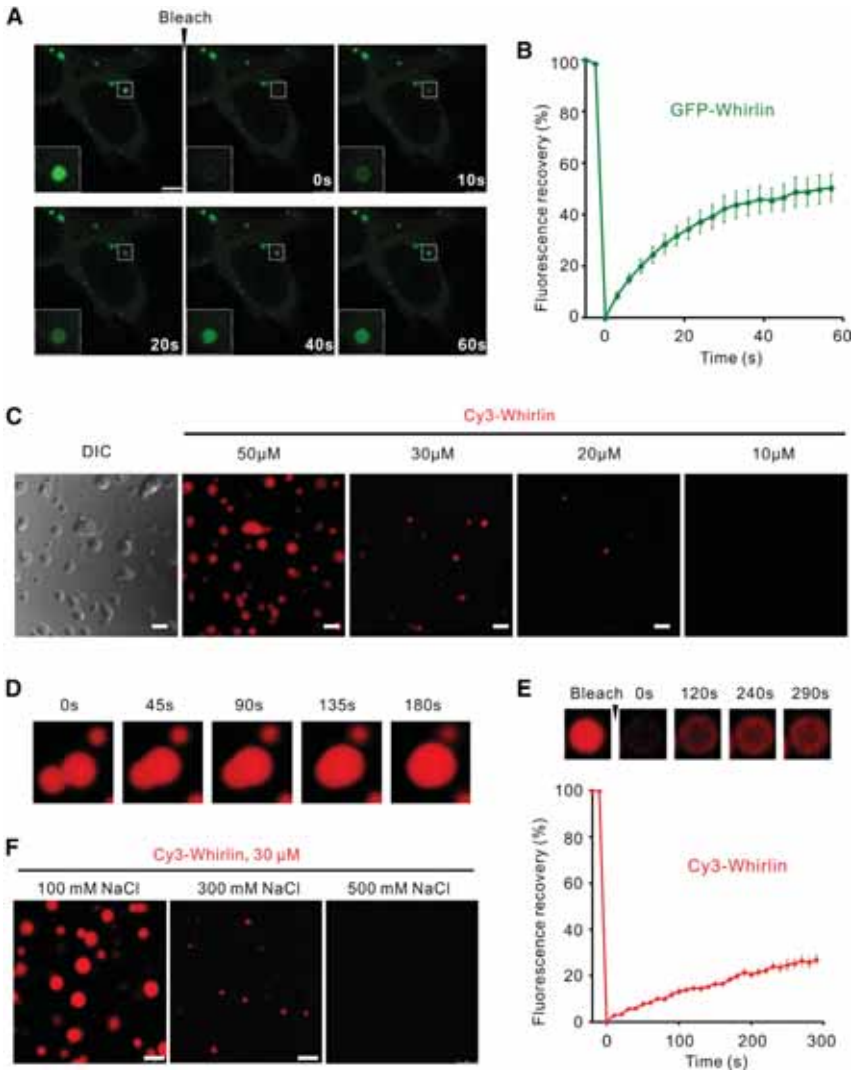

Figure 3. Whirlin undergoes phase separation *in vitro* and in living cells

(A) Representative images showing expression of GFP-Whirlin in HEK293T cells produced many spherical puncta. The FRAP experiment shows that GFP-Whirlin in the spherical puncta exchanged with those in cytoplasm. Scale bar: 5 μm.

(B) Quantitative results for FRAP experiment of GFP-Whirlin in puncta and cytoplasm of HEK293T cells. Time 0 refers to the time point of the photobleaching pulse. All data are represented as means ± SDs from 5 droplets (n = 5) in cells.

(C) DIC and fluorescence images showing purified full-length Whirlin protein underwent phase separation at indicated concentrations. Whirlin was sparsely labeled by Cy-3 at 1%. Scale bar: 5 μm.

(D) Representative images showing the Whirlin condensed droplets fused with one another over time.

(E) FRAP experiment of Cy3-Whirlin showing that the protein exchanged between the droplets and aqueous solution. Time 0 refers to the time point of the photobleaching pulse. All data are represented as means ± SDs from 5 independent experiments (N = 5).

(F) Fluorescence images showing the size and number of the Whirlin droplets were reduced with increased NaCl concentration. Scale bar: 5 μm.

See also Figure S3.

interactions are able to promote the formation of liquid-like condensates via phase separation (Shan et al., 2018; Zeng et al., 2016, 2018). Considering the multivalent interactions between Whirlin, Eps8, and Myo15, we wanted to investigate network complexity-dependent phase separation of the tip complex. Whirlin can only form visible sporadic droplets at 20 μM (Figure 4F). Eps8 PTB displayed oligomerization tendency when protein was concentrated, whereas Eps8 WBD did not (Figures S3A–S3C). A pull-down assay showed that Eps8 PTB interacts with itself to form oligomers (Figure S3D). Therefore, the addition of Eps8 would expand the valency of the system and promote the phase separation. As expected, the addition of Eps8 into Whirlin dramatically facilitated the phase separation of Whirlin (Figure 4F, top row, lane 2 versus lane 4). The liquid droplets appeared even at the concentration of 5 μM (Figure 4F). Unlike Eps8, Myo15, which lacks the oligomerization domain, did not significantly promote the phase separation of Whirlin (Figure 4F, top row, lane 3 versus lane 4). We concluded that Whirlin and Eps8 are the core components in the condensates and are less dynamic than Myo15, which may account for the observation that Myo15 appears to be more dynamic in FRAP assays (Figures 4C and 4E). These results demonstrated that the core components of the tip complex in stereocilia could form self-organized TCD-like assembly via phase separation driven by multivalent interactions in the complex (Figure 4G). Notably, Whirlin^{short} (which lacks the Eps8-binding domain), Eps8, and Myo15 did not form phase separation (Figure S4), most likely because the above-mentioned multivalent interactions were disrupted.

A deafness-associated mutation of Myo15 impairs the tip complex condensates

We wanted to find the possible relationship between the formation of TCD-like condensates and the pathogenesis of deafness. Several frameshift mutations of Myo15 that lack the intact PBM have been identified in deafness patients (Lezirovitz et al., 2008; Nal et al., 2007; Rehman et al., 2016). Specifically, a truncating mutation of Myo15 (p.S3525AfsX29, referred to as Myo15^{deaf} hereafter) lacks the very C-terminal PBM and instead bears an additional 28 residues (Lezirovitz et al., 2008; Figures 5A and S4). The Myo15^{deaf} mutant was expected to disrupt its binding to Whirlin PDZ3 due to the disrupted PBM. GST-Whirlin PDZ3 was unable to bind to Myo15^{deaf} as effectively as its wild-type counterpart (Figure 5B).

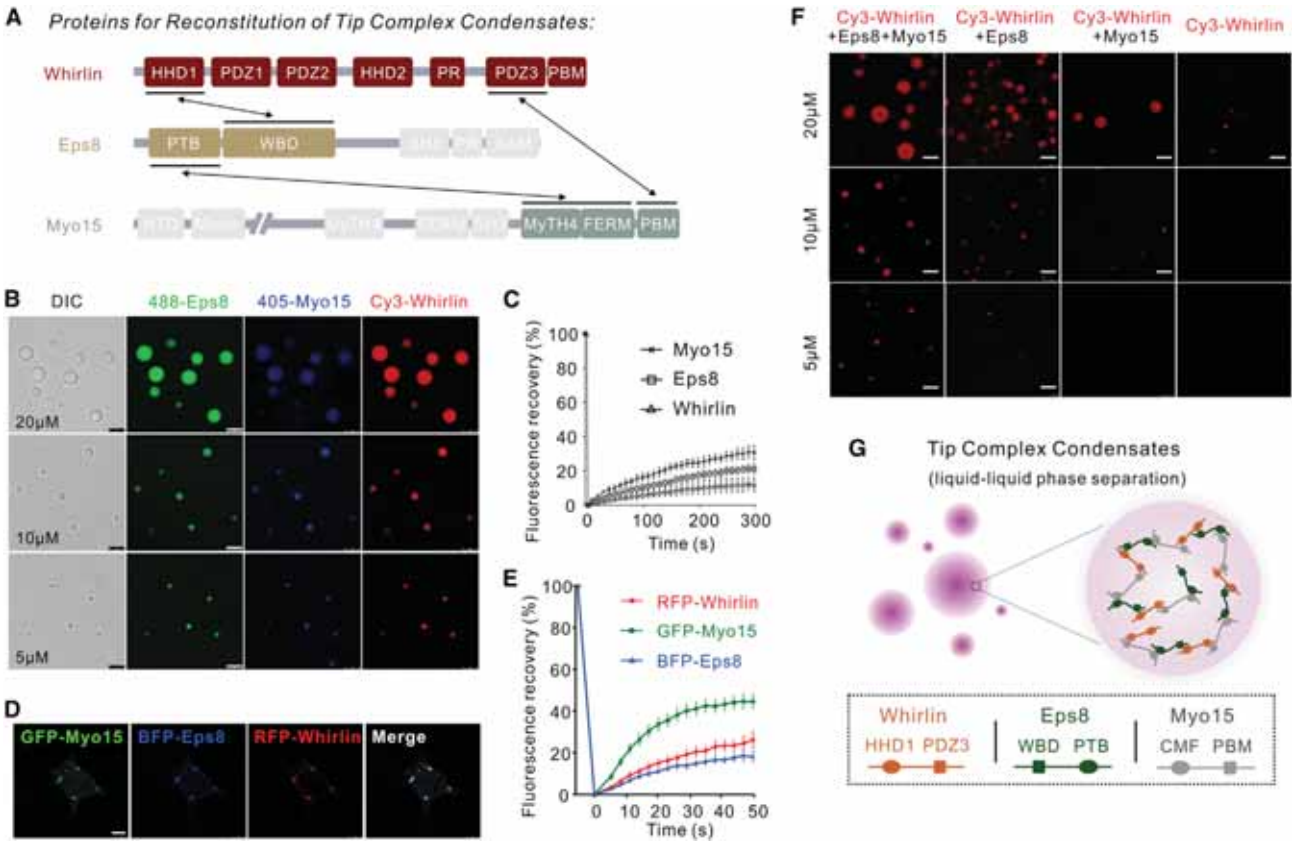

Figure 4. Formation of Whirlin-Myo15-Eps8 tip complex leads to TCD-like condensates

(A) Schematic diagram showing the components and the interactions among Whirlin, Myo15, and Eps8. Domains drawn in gray are removed from the corresponding proteins for technical reasons. Black arrows indicate the interactions between these proteins.

(B) DIC and fluorescence images showing that mixture of Whirlin, Myo15, and Eps8 at indicated concentrations led to formation of the liquid droplets. Whirlin, Myo15, and Eps8 were labeled with Cy3, Alexa 488, and Alexa-405, respectively, with each at 1% level. Scale bar: 5 μm.

(C) FRAP experiment showing the exchange kinetics of each protein between the tip complex condensates and dilute solution. All data are represented as means ± SDs from 5 independent experiments (N = 5).

(D) Representative images showing that co-expression of GFP-Myo15, RFP-Whirlin, and BFP-Eps8 in HEK293T cells produced multiple spherical puncta enriched with 3 proteins. Scale bar: 7.5 μm.

(E) FRAP experiment showing the exchange kinetics of each protein between the condensed puncta and dilute cytoplasm. All data are represented as means ± SDs from 5 droplets (n = 5) in cells.

(F) Valency- and protein concentration-dependent TCD-like condensates formation. Scale bar: 5 μm.

(G) A model depicting the mechanism of the formation of the TCD-like condensates via phase separation.

See also Figures S3, S4, and S7.

We next wanted to figure out how the deafness-associated Myo15 mutant affects the formation of the TCD-like condensates. We used a previously described sedimentation-based assay to quantify the distribution of the proteins in the bulk aqueous solutions (the "supernatant" fraction) and the condensed droplets (the "pellet" fraction) (Zeng et al., 2016; Zhu et al., 2020). In the wild-type tip complex mixture, ~95% of Whirlin and ~50% of Eps8 and Myo15 proteins were recovered from the condensed phase (Figures 5C and 5D). However, in the Myo15^{deaf} group, the number of proteins in the condensed droplets significantly decreased (only with ~50% of Whirlin and ~10% of Eps8 and Myo15 proteins) (Figures 5C and 5D). It is worth noting that all of the proteins used in the sedimentation-based assays were soluble and did not form aggregations in their *apo* forms (Figure S4). In addition, compared with the wild-type tip complex condensates, the ones with either Myo15^{deaf} or Myo15$^{\Delta PBM}$ showed fewer liquid droplets under microscopy (Figures 5E and 5F). These data indicated that the deafness-associated mutation of Myo15 leads to defective TCD-like condensate formation, most likely due to the impairment of multivalent interactions in the tip complex.

The tip complex condensates promote actin bundling

Little is known about how the components of the tip complex work together to orchestrate the regulation of actin dynamics in stereocilia, especially when some of them do not possess actin regulatory activity. Our reconstituted TCD-like condensates may provide some clues. In the reconstitution system,

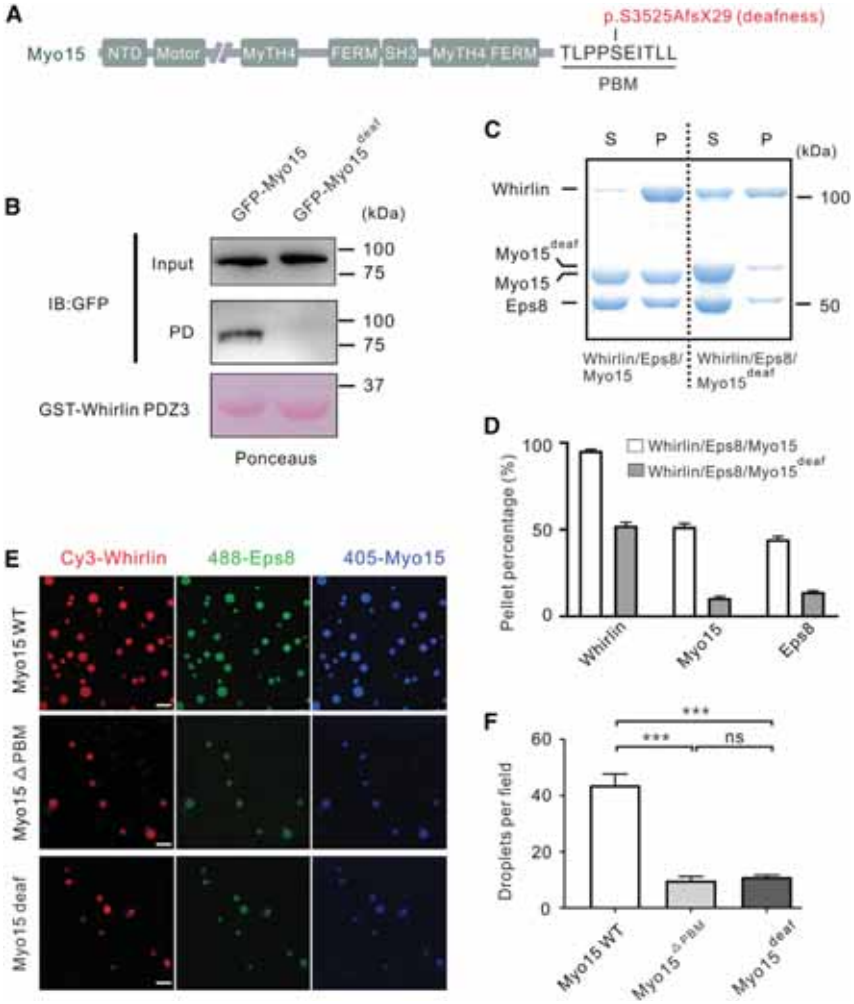

Figure 5. Deafness-associated mutation affects formation of the TCD-like condensates

(A) Domain organization of Myo15. Sequence of Myo15 PBM is shown. Deafness-causing mutation located at the PBM region of Myo15 is also listed.

(B) GST pull-down assay showing that Myo15^{deaf} failed to bind to Whirlin PDZ3.

(C) Representative SDS-PAGE analysis showing that Myo15^{deaf} impaired the formation of the liquid droplets in sedimentation-based assays. The concentration of each protein in this assay is 10 μM.

(D) Quantification data of (C). Results are expressed as means ± SDs from 3 independent batches of experiments.

(E) Representative fluorescence images showing that either Myo15^{deaf} or Myo15$^{\Delta PBM}$ showed fewer liquid droplets. The concentration of each protein in this assay is 20 μM. Scale bar: 10 μm.

(F) Quantification data of (E). Data are presented as means ± SEMs from 3 independent experiments using Student's t test (***p < 0.001; ns, not significant).

See also Figure S4.

only Eps8 is able to facilitate actin bundling via its C-terminal region, including the SH3, the proline-rich motifs, and the sterile alpha motif (SAM) domain (Disanza et al., 2004). Full-length Eps8 (Eps8^{FL}) alone induced the formation of actin bundles with a minimal effective concentration of 0.5 μM (Figure S5, with an actin:Eps8^{FL} molar ratio of 2:0.5), which is in line with the previous study (Disanza et al., 2006).

We next set up the actin bundling experiment in the presence of the tip complex condensates (Figure 6A). To this end, the tip complex mixture was incubated with pre-assembled F-actin, and then the actin bundling events were directly visualized under fluorescent microscopy (FM) or TEM (Figure 6A). In the tip complex mixture, the concentration of Eps8^{FL}, Myo15, and Whirlin were 0.25, 1.25, and 1.25 μM, respectively. Under such a condition, the mixture could effectively form condensed droplets (Figure S6). As expected, Eps8^{FL} alone could not induce actin bundling at the concentration of 0.25 μM (F-actin, 2 μM) (Figure 6B). Surprisingly, when the wild-type tip complex mixture was mixed with F-actin, long filamentous bundles were observed under FM (Figure 6B). The actin bundling event was also confirmed by the low-speed actin co-sedimentation assays (Figure S5). However, the tip complex mixture with the Myo15^{deaf} mutant showed limited actin bundling activity (Figure 6B), probably due to its reduced phase separation ability (Figure S6). Notably, the Myo15$^{\Delta PBM}$ mutant also displayed defective actin bundling activity (Figure 6B). As expected, the Whirlin-Eps8 mixture without Myo15 showed reduced actin bundles as well (Figure S5). Interestingly, wild-type Whirlin, Eps8^{FL}, and Myo15 colocalized into small consecutive puncta along with F-actin bundles (Figure 6C), suggesting that the condensed tip complex may act along the F-actin bundles. Furthermore, we used TEM to directly visualize actin bundles in the presence of the tip complex condensates. As expected, thick actin bundles were seen under TEM (the mean width was 301 ± 21 nm; the width of the thickest bundles was ~570 nm) (Figures 6D and 6E). In contrast, the tip complex mixture with the Myo15^{deaf} mutant exhibited much weaker actin crosslinking activity (the mean width was 144 ± 7 nm) than the wild-type group (Figures 6D and 6E). These results suggest that the formation of Whirlin-Eps8-Myo15 condensates may play a critical role in the promotion of actin bundle formation.

Discussion

Several electron-dense areas have been observed in hair cell stereocilia over 40 years. Examples are the TCD located at the tallest stereociliary tips, LTLD and UTLD situated at the lower and upper insertion sites of tip links, respectively, and the electron-dense materials at the lateral links and ankle links (Engström and Engström, 1978; Furness and Hackney, 1985; Hackney and Furness, 2013). Vast genetic and biochemical studies have

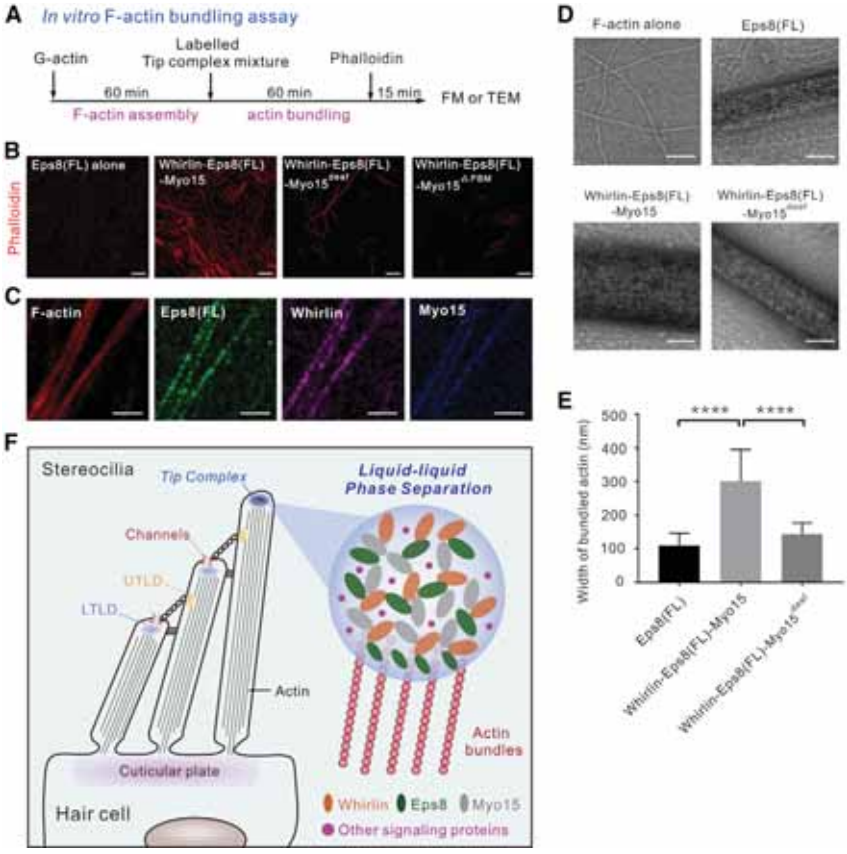

Figure 6. TCD-like condensates promote actin bundling

(A) A diagram showing the process of actin bundling experiment *in vitro*. FM, fluorescent microscopy; TEM, transmission electron microscopy.

(B) Representative images under FM showing that wild-type tip complex condensates significantly promote the actin bundling, whereas the mixture with Myo15^{deaf} or Myo15$^{\Delta PBM}$ could not. Scale bar: 5 μm.

(C) Representative images showing colocalization of Whirlin, Eps8, and Myo15 with F-actin bundles. Scale bar: 2.5 μm.

(D) Representative images of actin bundles induced by wild-type and mutant form of the tip complex mixture under TEM. Scale bar: 100 nm.

(E) Distribution of the width of actin bundles from the different groups of experiments. Statistics were performed by 2-tailed Student's t test. ****$p < 0.0001$.

(F) Proposed model for the tip density assembly mediated by phase separation of the tip complex. The tip complex including but not limited to Whirlin-Myo15-Eps8 axis may autonomously form condensed droplets in hair cell stereocilia via liquid-liquid phase separation. UTLD, upper tip link density; LTLD, lower tip link density.

See also Figures S5 and S6.

uncovered the molecular composition of these membrane-less electron densities. The TCD consists of various densely packed proteins (the tip complex), including scaffold proteins (e.g., Whirlin), molecular motors (e.g., Myo15, Myo3, Myo1), and actin regulatory proteins (e.g., Eps8, Espin) (Gillespie and Cyr, 2004; Salles et al., 2009). Recently, the polarity proteins LGN and Gαi were shown to form an ~200 nm nanodomain with Myo15 and Whirlin at the tips of the stereocilia (Mauriac et al., 2017; Tadenev et al., 2019). These proteins work together to regulate actin dynamics and stereocilia morphology. However, it remains unclear how this protein-dense semi-enclosed compartment is organized. Emerging evidence suggests that LLPS may be a general mechanism underlying the formation of membrane-less subcellular electron-dense plaques with broad physiological functions (Banani et al., 2017; Brangwynne et al., 2009; Hyman et al., 2014). For example, the PSD and the active zone in post- and presynapses of neurons, respectively, may be assembled through LLPS (Wu et al., 2019; Zeng et al., 2016, 2018).

In the present study, we demonstrate that Whirlin, Myo15, and Eps8, three major proteins in the TCD, can autonomously undergo phase separation and form highly dense but dynamic TCD-like condensates both *in vitro* and in living cells. Therefore, we provide evidence to show that the TCD in hair cell stereocilia may be formed via LLPS. Intriguingly, the Myo7A-USH1C-USH1G complex, the core components of UTLD, was recently shown to undergo phase separation as well (He et al., 2019). It was further proposed that UTLDs of stereocilia may be formed by the phase separation-mediated formation of the MYO7A-USH1C-USH1G condensates (He et al., 2019). It is noted that the formation of the UTLD-like condensates requires multivalent interactions between the tripartite complex, with a similar assembly mechanism in our work. At the tips of shorter/middle stereocilia where the LTLD was situated, Eps8 was essential for the initial elongation during development, while Eps8L2 was required for maintenance in adult hair cells (Furness et al., 2013). Eps8L2, an Eps8-like protein, shares a common modular organization with Eps8 and displays high sequence similarity with Eps8 (~50% aa identity) (Offenhäuser et al., 2004). The Whirlin-Myo15-Eps8L2 complex can also undergo phase separation (Figure S7). Therefore, it is most likely that the LTLD could also form through LLPS during both development and mature stages. These discoveries imply that the electron-dense areas observed in stereocilia (e.g., TCD, UTLD, LTLD, ankle-link complex) may form via phase separation. Future work is needed to verify this point.

What is the functional implication of the phase separation-mediated TCD condensates? We provide important clues by showing that *in vitro* reconstituted TCD-like condensates may effectively promote the actin bundling, although direct experimental evidence is required in stereocilia in future. Our fluorescent image data demonstrate that Whirlin, Eps8, and Myo15 display spotty-like, periodic co-puncta along bundled F-actin filaments, suggesting that the three proteins most likely form the condensates via LLPS to promote actin bundling. However, it cannot be ruled out that the condensates may exist as a gel-

like or solid state, which is difficult to investigate at this stage. Future work is needed to address this issue. Since Eps8 alone could not induce actin bundling at lower concentrations (Figure S5), it is possible that the TCD-like condensates facilitate the actin bundling by concentrating Eps8 in the mixture. Thus, it would not be surprising that the mutants of Myo15 that impair the formation of the TCD-like condensates led to defects in actin bundling activity (Figure 6). These data indicate that the LLPS-mediated TCD condensates may play critical roles in the regulation of stereocilia morphology by concentrating actin regulatory proteins in hair cells (Figure 6F). In accordance with this conclusion, it is generally believed that LLPS is used by cells to concentrate biomolecules at specific subcellular compartments (Banani et al., 2017; Shin and Brangwynne, 2017; Zhu et al., 2020). Intriguingly, Whirlin was reported to interact with actin-free Espin, another actin crosslinking protein, at the ankle links and stereocilia tips in hair cells (Wang et al., 2012). This interaction accelerated the exchange between pools of actin-free Espin and actin-bound Espin and may indirectly weaken the cross-links of Espin with actin filaments (Wang et al., 2012). The two mechanisms used by Whirlin (Whirlin-Espin axis and Whirlin-Eps8-Myo15 axis) to regulate actin dynamics are obviously different. These data strongly suggest that Whirlin, a versatile organizer of actin dynamics, may coordinate and balance multiple signaling pathways to precisely regulate actin dynamics in different compartments of stereocilia and/or different stages of stereocilia development.

Actin-based protrusions, including stereocilia, filopodia, and microvilli, serve a huge variety of functions in eukaryotic cells (Sahin et al., 2005). When comparing the three types of actin protrusions, the most intriguing commonality is the presence of the condensed tip complex density at the distal tips of these protrusions (Sahin et al., 2005). In filopodia and microvilli, the dense matrix contains actin polymerization proteins (e.g., VASP, Formins), actin bundling proteins (e.g., Fascin, Espin, villin, Eps8), myosins, and other signaling proteins (Breitsprecher et al., 2008; Harker et al., 2019; Kerber and Cheney, 2011; Postema et al., 2018; Sahin et al., 2005; Schirenbeck et al., 2005). It will be interesting to test whether the tip density of filopodia and microvilli could also be formed by phase separation.

STAR★METHODS

Detailed methods are provided in the online version of this paper and include the following:

- KEY RESOURCES TABLE
- RESOURCE AVAILABILITY
  - Lead contact
  - Materials availability
  - Data and code availability
- EXPERIMENTAL MODEL AND SUBJECT DETAILS
  - Bacterial strain
  - Cell Culture
- METHOD DETAILS
  - Protein expression and purification
  - GST-pull down assay
  - Fluorescence polarization assay
  - Crystallization, data collection and structure determination
  - Cellular localization assay
  - Protein labeling with fluorophore
  - *In vitro* phase separation assay
  - Fluorescence recovery after photo-bleaching assay
  - *In vitro* actin polymerization and bundling assay
- QUANTIFICATION AND STATISTICAL ANALYSIS

SUPPLEMENTAL INFORMATION

Supplemental Information can be found online at https://doi.org/10.1016/j.celrep.2021.108770.

ACKNOWLEDGMENTS

We thank beamlines BL18U1 and BL19U1 at Shanghai Synchrotron Radiation Facility (SSRF, China) and BL41XU at Spring-8 (Hyogo, Japan) for X-ray beam time; the staff members of the Large-scale Protein Preparation System and Molecular Imaging System at the National Facility for Protein Science in Shanghai (NFPS), Zhangjiang Lab, China, for providing technical support and assistance in data collection and analysis; Dr. Wenyu Wen for providing assistance in the data collection of fluorescence polarization assay; and Dr. Xiuna Yang for her help in taking EM images. This work was supported by grants from the National Key R&D Program of China (2017YFA0504901 to R.Z. and 2018YFA0507900 to J.Z.), grants from the National Natural Science Foundation of China (U2032122 and 31770779 to J.Z., 31670734 and 91953110 to C.W., and 31900858 to Q.L.), a grant from Science and Technology Commission of Shanghai Municipality (20S11900200 to J.Z.), grants from USTC Research Funds of Double First-Class Initiative: YD9100002006 and the Fundamental Research Funds for the Central Universities: WK9100000029 to C.W., and a grant from the Chief Scientist Program of Shanghai Institutes for Biological Sciences, Chinese Academy of Sciences to R.Z.

AUTHOR CONTRIBUTIONS

J.Z., L.L., and Y.S. designed the experiments; L.L., Y.S., and M.W. performed the experiments; L.L. and Y.S. carried out the X-ray data collection and structure determination; J.Z., L.L., Y.S., M.W., C.W., Q.L., and R.Z. analyzed the data; L.L. and J.Z. drafted the manuscript; all of the authors commented on the manuscript; and J.Z. coordinated the project.

DECLARATION OF INTERESTS

The authors declare no competing interests.

Received: February 12, 2020
Revised: January 5, 2021
Accepted: January 28, 2021
Published: February 23, 2021

REFERENCES

Adams, P.D., Afonine, P.V., Bunkóczi, G., Chen, V.B., Davis, I.W., Echols, N., Headd, J.J., Hung, L.W., Kapral, G.J., Grosse-Kunstleve, R.W., et al. (2010). PHENIX: a comprehensive Python-based system for macromolecular structure solution. Acta Crystallogr. D Biol. Crystallogr. *66*, 213–221.

Banani, S.F., Lee, H.O., Hyman, A.A., and Rosen, M.K. (2017). Biomolecular condensates: organizers of cellular biochemistry. Nat. Rev. Mol. Cell Biol. *18*, 285–298.

Barr-Gillespie, P.G. (2015). Assembly of hair bundles, an amazing problem for cell biology. Mol. Biol. Cell *26*, 2727–2732.

Behlouli, A., Bonnet, C., Abdi, S., Bouaita, A., Lelli, A., Hardelin, J.P., Schietroma, C., Rous, Y., Louha, M., Cheknane, A., et al. (2014). EPS8, encoding

an actin-binding protein of cochlear hair cell stereocilia, is a new causal gene for autosomal recessive profound deafness. Orphanet J. Rare Dis. *9*, 55.

Belyantseva, I.A., Boger, E.T., and Friedman, T.B. (2003). Myosin XVa localizes to the tips of inner ear sensory cell stereocilia and is essential for staircase formation of the hair bundle. Proc. Natl. Acad. Sci. USA *100*, 13958–13963.

Belyantseva, I.A., Boger, E.T., Naz, S., Frolenkov, G.I., Sellers, J.R., Ahmed, Z.M., Griffith, A.J., and Friedman, T.B. (2005). Myosin-XVa is required for tip localization of whirlin and differential elongation of hair-cell stereocilia. Nat. Cell Biol. *7*, 148–156.

Boughman, J.A., Vernon, M., and Shaver, K.A. (1983). Usher syndrome: definition and estimate of prevalence from two high-risk populations. J. Chronic Dis. *36*, 595–603.

Brangwynne, C.P., Eckmann, C.R., Courson, D.S., Rybarska, A., Hoege, C., Gharakhani, J., Jülicher, F., and Hyman, A.A. (2009). Germline P granules are liquid droplets that localize by controlled dissolution/condensation. Science *324*, 1729–1732.

Breitsprecher, D., Kiesewetter, A.K., Linkner, J., Urbanke, C., Resch, G.P., Small, J.V., and Faix, J. (2008). Clustering of VASP actively drives processive, WH2 domain-mediated actin filament elongation. EMBO J. *27*, 2943–2954.

Chen, Q., Zou, J., Shen, Z., Zhang, W., and Yang, J. (2014). Whirlin and PDZ domain-containing 7 (PDZD7) proteins are both required to form the quaternary protein complex associated with Usher syndrome type 2. J. Biol. Chem. *289*, 36070–36088.

Delprat, B., Michel, V., Goodyear, R., Yamasaki, Y., Michalski, N., El-Amraoui, A., Perfettini, I., Legrain, P., Richardson, G., Hardelin, J.P., and Petit, C. (2005). Myosin XVa and whirlin, two deafness gene products required for hair bundle growth, are located at the stereocilia tips and interact directly. Hum. Mol. Genet. *14*, 401–410.

Disanza, A., Carlier, M.F., Stradal, T.E., Didry, D., Frittoli, E., Confalonieri, S., Croce, A., Wehland, J., Di Fiore, P.P., and Scita, G. (2004). Eps8 controls actin-based motility by capping the barbed ends of actin filaments. Nat. Cell Biol. *6*, 1180–1188.

Disanza, A., Mantoani, S., Hertzog, M., Gerboth, S., Frittoli, E., Steffen, A., Berhoerster, K., Kreienkamp, H.J., Milanesi, F., Di Fiore, P.P., et al. (2006). Regulation of cell shape by Cdc42 is mediated by the synergic actin-bundling activity of the Eps8-IRSp53 complex. Nat. Cell Biol. *8*, 1337–1347.

Drummond, M.C., Belyantseva, I.A., Friderici, K.H., and Friedman, T.B. (2012). Actin in hair cells and hearing loss. Hear. Res. *288*, 89–99.

Emsley, P., and Cowtan, K. (2004). Coot: model-building tools for molecular graphics. Acta Crystallogr. D Biol. Crystallogr. *60*, 2126–2132.

Engström, H., and Engström, B. (1978). Structure of the hairs on cochlear sensory cells. Hear. Res. *1*, 49–66.

Furness, D.N., and Hackney, C.M. (1985). Cross-links between stereocilia in the guinea pig cochlea. Hear. Res. *18*, 177–188.

Furness, D.N., Johnson, S.L., Manor, U., Rüttiger, L., Tocchetti, A., Offenhauser, N., Olt, J., Goodyear, R.J., Vijayakumar, S., Dai, Y., et al. (2013). Progressive hearing loss and gradual deterioration of sensory hair bundles in the ears of mice lacking the actin-binding protein Eps8L2. Proc. Natl. Acad. Sci. USA *110*, 13898–13903.

Gillespie, P.G., and Cyr, J.L. (2004). Myosin-1c, the hair cell's adaptation motor. Annu. Rev. Physiol. *66*, 521–545.

Gillespie, P.G., and Müller, U. (2009). Mechanotransduction by hair cells: models, molecules, and mechanisms. Cell *139*, 33–44.

Hackney, C.M., and Furness, D.N. (2013). The composition and role of cross links in mechanoelectrical transduction in vertebrate sensory hair cells. J. Cell Sci. *126*, 1721–1731.

Harker, A.J., Katkar, H.H., Bidone, T.C., Aydin, F., Voth, G.A., Applewhite, D.A., and Kovar, D.R. (2019). Ena/VASP processive elongation is modulated by avidity on actin filaments bundled by the filopodia cross-linker fascin. Mol. Biol. Cell *30*, 851–862.

He, Y., Li, J., and Zhang, M. (2019). Myosin VII, USH1C, and ANKS4B or USH1G Together Form Condensed Molecular Assembly via Liquid-Liquid Phase Separation. Cell Rep. *29*, 974–986.e4.

Hertzog, M., Milanesi, F., Hazelwood, L., Disanza, A., Liu, H., Perlade, E., Malabarba, M.G., Pasqualato, S., Maiolica, A., Confalonieri, S., et al. (2010). Molecular basis for the dual function of Eps8 on actin dynamics: bundling and capping. PLoS Biol. *8*, e1000387.

Hyman, A.A., Weber, C.A., and Jülicher, F. (2014). Liquid-liquid phase separation in biology. Annu. Rev. Cell Dev. Biol. *30*, 39–58.

Kabsch, W. (2010). Xds. Acta Crystallogr. D Biol. Crystallogr. *66*, 125–132.

Kachar, B., Parakkal, M., Kurc, M., Zhao, Y., and Gillespie, P.G. (2000). High-resolution structure of hair-cell tip links. Proc. Natl. Acad. Sci. USA *97*, 13336–13341.

Keats, B.J., and Corey, D.P. (1999). The usher syndromes. Am. J. Med. Genet. *89*, 158–166.

Kerber, M.L., and Cheney, R.E. (2011). Myosin-X: a MyTH-FERM myosin at the tips of filopodia. J. Cell Sci. *124*, 3733–3741.

Kikkawa, Y., Mburu, P., Morse, S., Kominami, R., Townsend, S., and Brown, S.D. (2005). Mutant analysis reveals whirlin as a dynamic organizer in the growing hair cell stereocilium. Hum. Mol. Genet. *14*, 391–400.

Lezirovitz, K., Pardono, E., de Mello Auricchio, M.T., de Carvalho E Silva, F.L., Lopes, J.J., Abreu-Silva, R.S., Romanos, J., Batissoco, A.C., and Mingroni-Netto, R.C. (2008). Unexpected genetic heterogeneity in a large consanguineous Brazilian pedigree presenting deafness. Eur. J. Hum. Genet. *16*, 89–96.

Manor, U., Disanza, A., Grati, M., Andrade, L., Lin, H., Di Fiore, P.P., Scita, G., and Kachar, B. (2011). Regulation of stereocilia length by myosin XVa and whirlin depends on the actin-regulatory protein Eps8. Curr. Biol. *21*, 167–172.

Mathur, P.D., and Yang, J. (2019). Usher syndrome and non-syndromic deafness: functions of different whirlin isoforms in the cochlea, vestibular organs, and retina. Hear. Res. *375*, 14–24.

Mauriac, S.A., Hien, Y.E., Bird, J.E., Carvalho, S.D., Peyroutou, R., Lee, S.C., Moreau, M.M., Blanc, J.M., Geyser, A., Medina, C., et al. (2017). Defective Gpsm2/Gα_{i3} signalling disrupts stereocilia development and growth cone actin dynamics in Chudley-McCullough syndrome. Nat. Commun. *8*, 14907.

Mburu, P., Mustapha, M., Varela, A., Weil, D., El-Amraoui, A., Holme, R.H., Rump, A., Hardisty, R.E., Blanchard, S., Coimbra, R.S., et al. (2003). Defects in whirlin, a PDZ domain molecule involved in stereocilia elongation, cause deafness in the whirler mouse and families with DFNB31. Nat. Genet. *34*, 421–428.

McCoy, A.J., Grosse-Kunstleve, R.W., Adams, P.D., Winn, M.D., Storoni, L.C., and Read, R.J. (2007). Phaser crystallographic software. J. Appl. Cryst. *40*, 658–674.

Michalski, N., and Petit, C. (2019). Genes Involved in the Development and Physiology of Both the Peripheral and Central Auditory Systems. Annu. Rev. Neurosci. *42*, 67–86.

Mogensen, M.M., Rzadzinska, A., and Steel, K.P. (2007). The deaf mouse mutant whirler suggests a role for whirlin in actin filament dynamics and stereocilia development. Cell Motil. Cytoskeleton *64*, 496–508.

Nal, N., Ahmed, Z.M., Erkal, E., Alper, O.M., Lüleci, G., Dinç, O., Waryah, A.M., Ain, Q., Tasneem, S., Husnain, T., et al. (2007). Mutational spectrum of MYO15A: the large N-terminal extension of myosin XVA is required for hearing. Hum. Mutat. *28*, 1014–1019.

Offenhäuser, N., Borgonovo, A., Disanza, A., Romano, P., Ponzanelli, I., Iannolo, G., Di Fiore, P.P., and Scita, G. (2004). The eps8 family of proteins links growth factor stimulation to actin reorganization generating functional redundancy in the Ras/Rac pathway. Mol. Biol. Cell *15*, 91–98.

Palay, S.L. (1956). Synapses in the central nervous system. J. Biophys. Biochem. Cytol. *2* (*4, Suppl*), 193–202.

Petit, C., and Richardson, G.P. (2009). Linking genes underlying deafness to hair-bundle development and function. Nat. Neurosci. *12*, 703–710.

Postema, M.M., Grega-Larson, N.E., Neininger, A.C., and Tyska, M.J. (2018). IRTKS (BAIAP2L1) Elongates Epithelial Microvilli Using EPS8-Dependent and Independent Mechanisms. Curr. Biol. *28*, 2876–2888.e4.

Potterton, E., Briggs, P., Turkenburg, M., and Dodson, E. (2003). A graphical user interface to the CCP4 program suite. Acta Crystallogr. D Biol. Crystallogr. *59*, 1131–1137.

Probst, F.J., Fridell, R.A., Raphael, Y., Saunders, T.L., Wang, A., Liang, Y., Morell, R.J., Touchman, J.W., Lyons, R.H., Noben-Trauth, K., et al. (1998). Correction of deafness in shaker-2 mice by an unconventional myosin in a BAC transgene. Science *280*, 1444–1447.

Rehman, A.U., Bird, J.E., Faridi, R., Shahzad, M., Shah, S., Lee, K., Khan, S.N., Imtiaz, A., Ahmed, Z.M., Riazuddin, S., et al. (2016). Mutational Spectrum of MYO15A and the Molecular Mechanisms of DFNB3 Human Deafness. Hum. Mutat. *37*, 991–1003.

Richardson, G.P., and Petit, C. (2019). Hair-Bundle Links: Genetics as the Gateway to Function. Cold Spring Harb. Perspect. Med. *9*, a033142.

Rzadzinska, A.K., Schneider, M.E., Davies, C., Riordan, G.P., and Kachar, B. (2004). An actin molecular treadmill and myosins maintain stereocilia functional architecture and self-renewal. J. Cell Biol. *164*, 887–897.

Sahin, M., Greer, P.L., Lin, M.Z., Poucher, H., Eberhart, J., Schmidt, S., Wright, T.M., Shamah, S.M., O'connell, S., Cowan, C.W., et al. (2005). Eph-dependent tyrosine phosphorylation of ephexin1 modulates growth cone collapse. Neuron *46*, 191–204.

Sakaguchi, H., Tokita, J., Müller, U., and Kachar, B. (2009). Tip links in hair cells: molecular composition and role in hearing loss. Curr. Opin. Otolaryngol. Head Neck Surg. *17*, 388–393.

Salles, F.T., Merritt, R.C., Jr., Manor, U., Dougherty, G.W., Sousa, A.D., Moore, J.E., Yengo, C.M., Dosé, A.C., and Kachar, B. (2009). Myosin IIIa boosts elongation of stereocilia by transporting espin 1 to the plus ends of actin filaments. Nat. Cell Biol. *11*, 443–450.

Schirenbeck, A., Bretschneider, T., Arasada, R., Schleicher, M., and Faix, J. (2005). The Diaphanous-related formin dDia2 is required for the formation and maintenance of filopodia. Nat. Cell Biol. *7*, 619–625.

Shan, Z., Tu, Y., Yang, Y., Liu, Z., Zeng, M., Xu, H., Long, J., Zhang, M., Cai, Y., and Wen, W. (2018). Basal condensation of Numb and Pon complex via phase transition during Drosophila neuroblast asymmetric division. Nat. Commun. *9*, 737.

Shin, Y., and Brangwynne, C.P. (2017). Liquid phase condensation in cell physiology and disease. Science *357*, eaaf4382.

Tadenev, A.L.D., Akturk, A., Devanney, N., Mathur, P.D., Clark, A.M., Yang, J., and Tarchini, B. (2019). GPSM2-GNAI Specifies the Tallest Stereocilia and Defines Hair Bundle Row Identity. Curr. Biol. *29*, 921–934.e4.

van Wijk, E., van der Zwaag, B., Peters, T., Zimmermann, U., Te Brinke, H., Kersten, F.F., Märker, T., Aller, E., Hoefsloot, L.H., Cremers, C.W., et al. (2006). The DFNB31 gene product whirlin connects to the Usher protein network in the cochlea and retina by direct association with USH2A and VLGR1. Hum. Mol. Genet. *15*, 751–765.

Wang, A., Liang, Y., Fridell, R.A., Probst, F.J., Wilcox, E.R., Touchman, J.W., Morton, C.C., Morell, R.J., Noben-Trauth, K., Camper, S.A., and Friedman, T.B. (1998). Association of unconventional myosin MYO15 mutations with human nonsyndromic deafness DFNB3. Science *280*, 1447–1451.

Wang, L., Zou, J., Shen, Z., Song, E., and Yang, J. (2012). Whirlin interacts with espin and modulates its actin-regulatory function: an insight into the mechanism of Usher syndrome type II. Hum. Mol. Genet. *21*, 692–710.

Wright, P.E., and Dyson, H.J. (2015). Intrinsically disordered proteins in cellular signalling and regulation. Nat. Rev. Mol. Cell Biol. *16*, 18–29.

Wu, X., Cai, Q., Shen, Z., Chen, X., Zeng, M., Du, S., and Zhang, M. (2019). RIM and RIM-BP Form Presynaptic Active-Zone-like Condensates via Phase Separation. Mol. Cell *73*, 971–984.e5.

Zampini, V., Rüttiger, L., Johnson, S.L., Franz, C., Furness, D.N., Waldhaus, J., Xiong, H., Hackney, C.M., Holley, M.C., Offenhauser, N., et al. (2011). Eps8 regulates hair bundle length and functional maturation of mammalian auditory hair cells. PLoS Biol. *9*, e1001048.

Zeng, M., Shang, Y., Araki, Y., Guo, T., Huganir, R.L., and Zhang, M. (2016). Phase Transition in Postsynaptic Densities Underlies Formation of Synaptic Complexes and Synaptic Plasticity. Cell *166*, 1163–1175.e12.

Zeng, M., Chen, X., Guan, D., Xu, J., Wu, H., Tong, P., and Zhang, M. (2018). Reconstituted Postsynaptic Density as a Molecular Platform for Understanding Synapse Formation and Plasticity. Cell *174*, 1172–1187.e16.

Zhang, M., and Wang, W. (2003). Organization of signaling complexes by PDZ-domain scaffold proteins. Acc. Chem. Res. *36*, 530–538.

Zhu, J., Shang, Y., and Zhang, M. (2016). Mechanistic basis of MAGUK-organized complexes in synaptic development and signalling. Nat. Rev. Neurosci. *17*, 209–223.

Zhu, J., Zhou, Q., Xia, Y., Lin, L., Li, J., Peng, M., Zhang, R., and Zhang, M. (2020). GIT/PIX Condensates Are Modular and Ideal for Distinct Compartmentalized Cell Signaling. Mol. Cell *79*, 782–796.e6.